On the plug potential formation mechanism in a tandem mirror

I. Katanuma,[a] Y. Tatematsu, K. Ishii, T. Saito, and K. Yatsu
Plasma Research Center, University of Tsukuba, Tsukuba-City 305-8577, Japan

(Received 6 November 2001; accepted 6 May 2002)

A formation mechanism of the plug potential in a tandem mirror is proposed. The orbits for ions, which are accelerated by the thermal barrier potential, are calculated numerically in a magnetic mirror field. A non-Maxwellian electron distribution function, which leads to a modified Boltzmann law, is assumed in order to determine the electrostatic potential profile. Monte Carlo simulation is carried out for ion dynamics to include the effects of Coulomb collisions and ion radial losses. It is found that the plug potential is formed under the condition that the ions trapped in the thermal barrier region are few. © *2002 American Institute of Physics.* [DOI: 10.1063/1.1489424]

I. INTRODUCTION

The problem of an electrostatic potential along magnetic field lines has been recognized as an important issue in plasma physics and efforts to understand the mechanism of an electrostatic potential formation have been made. In space plasmas, for example, an electrostatic potential formation mechanism is proposed by Ref. 1, where the field-aligned electrostatic potential is supposed to be generated by the different pitch angle anisotropy of ions and electrons. The idea has also been applied to more complicated problems.[2–4] An essential point for field-aligned electrostatic potential formation is that there exists an electron current along magnetic field lines in space plasmas. Recent calculations of potential formation are based on the assumption of the existence of an electron current along magnetic field lines.[5]

The electrostatic potential for trapping particles is utilized in a wide area, not only neutral plasmas and non-neutral plasmas[6] but also a field of antihydrogen,[7–9] where antiprotons and positrons are trapped in the electrostatic potential in a minimum-*B* magnetic mirror.

The tandem mirror tries to make use of a field-aligned electrostatic potential for ion confinement.[10–12] The original scenario to create an electrostatic potential hill at a midway point from the thermal barrier region to the outer mirror throat, where the potential hill is called the ion confining potential or plug potential, included a magnetically trapped high energy ion population (sloshing ions) in the end mirror cells of a tandem mirror. However, subsequent experiments revealed that the formation of the plug potential did not require the sloshing ions.[13,14] That is, only electron cyclotron resonance heating (ECRH) applied in the plug region can be responsible for the plug potential formation.

In the end mirror cells of a tandem mirror there is no electron flow in the steady state, so the mechanism of the plug potential formation is different from the field-aligned electrostatic potential formation in space plasmas, such as the magnetosphere.

Efforts at understanding the mechanism of the plug potential formation have been reported.[15–19] It has been shown that the ions accelerated by the thermal barrier potential and the non-Maxwellian electrons create the plug potential. However, it was found that the plug potential formation requires a population of ions in the loss cone region in velocity space, in addition to passing ions from the central cell and ions trapped in the thermal barrier potential, as will be mentioned in Sec. II.

Previous works[16–19] include the ionization effects for a production of ions in the loss cone region in velocity space. The ionization rate required for the plug potential formation, however, is one ordered magnitude larger than that measured in a present tandem mirror experiment.[19] The purpose of this article, therefore, is to make the mechanism of the plug potential formation clear by including Coulomb pitch-angle scattering of ions instead of ionization, where Coulomb collisions scatter ions in the passing region and the trapped region in velocity space into the loss cone region.

In Sec. II a modified Boltzmann law is derived from a non-Maxwellian electron distribution function. The Monte Carlo simulations are carried out to study a plug potential formation in Sec. III. A summary is given in Sec. IV.

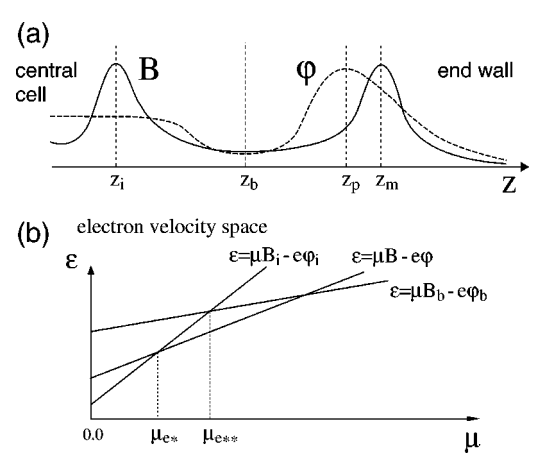

FIG. 1. Schematic diagram of the end mirror cell in a tandem mirror (a) and the electron velocity space represented by ε and μ (b).

[a]Electronic mail: katanuma@prc.tsukuba.ac.jp

II. SIMPLE ANALYSIS

A Maxwellian electron distribution function leads to the conventional Boltzmann law of an electrostatic potential, where a local maximum point of the electrostatic potential locates at the local maximum point of the electron density along a magnetic field line. The local maximum point of the electrostatic potential, however, is not the same as that of the electron axial density in a tandem mirror, so that we consider the non-Maxwellian electron distribution function in the following.

The electrons coming from the central cell are reflected by the thermal barrier potential and only a few of the electrons reach the plug region. On the other hand, the electrons magnetically trapped in the plug/barrier region are heated by ECRH.

The schematic diagram of electrostatic potential and magnetic field profiles are shown in Fig. 1(a), and the velocity space of electrons is shown in Fig. 1(b). While the electrons are Maxwellian at $z=z_i$, where electrons are supplied from the central cell, the electrons trapped in the plug/barrier region are assumed to be non-Maxwellian, the distribution function of which is written as

$$f_e=\begin{cases} n_{ec}\left(\dfrac{m_e}{2\pi T_{ec}}\right)^{3/2}\exp\left\{-\dfrac{\varepsilon+e\varphi_i}{T_{ec}}\right\} & \text{for } \varepsilon\geqslant\mu B_i-e\varphi_i \\ n_{ec}\left(\dfrac{m_e}{2\pi T_{ec}}\right)^{3/2}\exp\left\{-\dfrac{\varepsilon+e\varphi_i-\alpha_e\mu B_i}{(1-\alpha_e)T_{ec}}\right\} & \text{for } \varepsilon<\mu B_i-e\varphi_i. \end{cases} \tag{1}$$

Here α_e is constant, T_{ec} and n_{ec} are the electron temperature and density at $z=z_i$, m_e is electron mass, and e is unit charge. The notations B and φ represent the magnetic field strength and electrostatic potential, the subscript i denotes the quantity at $z=z_i$. The quantities ε and μ are the electron total energy ($\varepsilon=\frac{1}{2}m_e v^2-e\varphi$) and magnetic moment ($\mu=\frac{1}{2}m_e v_\perp^2/B$), where v is velocity, and $v_\perp$ is the velocity component perpendicular to the magnetic field. Equation (1) is applied in the region $z_b\leqslant z\leqslant z_m$ in Fig. 1(a). The distribution function (1) is the simplest one which includes the effect of non-Maxwellian electrons trapped magnetically but is able to be integrated analytically in velocity space. This is the reason we adopt Eq. (1) as the electron distribution function in the end-mirror cell.

In previous works[16–19] the electron velocity space was divided into two pieces by the line $\varepsilon=\mu B_b-e\varphi_b$, where electrons trapped electrostatically in the plug potential are considered. The density obtained in the previous calculation[16–19] increases gradually from the thermal barrier to the outer mirror throat, while the density at the plug is smaller than that at the thermal barrier in the actual experiments.

In this article, the electron velocity space is divided by the line $\varepsilon=\mu B_i-e\varphi_i$ in Eq. (1), where electrons trapped magnetically in the thermal barrier region are considered. Another reason to pay attention to the electrons trapped magnetically in the thermal barrier region, but not the ones trapped electrostatically in the plug potential, is that the formation of the plug potential accompanies the thermal barrier potential formation.[20] The distribution function of electrons trapped in the plug, therefore, is the same as that of electrons trapped magnetically in the thermal barrier region.

The electron density $n_e(z)$ ($z_b\leqslant z\leqslant z_m$) is given as

$$n_e(z)=\frac{Bn_{ec}}{\sqrt{\pi}T_{ec}^{3/2}}\left(\left[\int_{\mu B_b-e\varphi_b}^{\infty}d\varepsilon\int_0^{\mu_{e**}}d\mu+\int_{\mu B_i-e\varphi_i}^{\infty}d\varepsilon\int_{\mu_{e**}}^{\infty}d\mu\right]\frac{1}{(\varepsilon-\mu B+e\varphi)^{1/2}}\exp\left\{-\frac{\varepsilon+e\varphi_i}{T_{ec}}\right\}\right.$$
$$\left.+\int_{\mu B-e\varphi}^{\mu B_i-e\varphi_i}d\varepsilon\int_{\mu_{e*}}^{\infty}d\mu\frac{1}{(\varepsilon-\mu B+e\varphi)^{1/2}}\exp\left\{-\frac{\varepsilon+e\varphi_i-\alpha_e\mu B_i}{(1-\alpha_e)T_{ec}}\right\}\right). \tag{2}$$

Here $\mu_{e*}\equiv e(\varphi-\varphi_i)/(B-B_i)$ and $\mu_{e**}\equiv e(\varphi_b-\varphi_i)/(B_b-B_i)$. The integrations in Eq. (2) are carried out to be

$$n_e(z) \simeq \begin{cases} n_{ec}\dfrac{B(1-\alpha_e)}{(B-\alpha_e B_i)}\left(\dfrac{B_i-B}{B_i}\right)^{1/2}\exp\left\{-\dfrac{B_i}{(B-B_i)}\dfrac{e(\varphi-\varphi_i)}{T_{ec}}\right\} \\ \quad \text{in case of} \quad \varphi \leqslant \varphi_i \\ n_{ec}\dfrac{B(1-\alpha_e)}{(B-\alpha_e B_i)}\left(\dfrac{B_i-B}{B_i}\right)^{1/2}\exp\left\{-\dfrac{B_i}{(B-B_i)}\dfrac{e(\varphi-\varphi_i)}{T_{ec}}\right\} \\ \quad \text{in case of} \quad 1 \gtrsim \dfrac{B_i}{(B_i-B)}\dfrac{e(\varphi-\varphi_i)}{T_{ec}} > 0 \\ \begin{cases} n_{ec}\dfrac{B(1-\alpha_e)^{3/2}}{(B-\alpha_e B_i)}\exp\left\{\dfrac{e(\varphi-\varphi_i)}{(1-\alpha_e)T_{ec}}\right\} & \text{for} \quad (1-\alpha_e)>0 \\ n_{ec}\dfrac{B(\alpha_e-1)}{B_i}\dfrac{1}{\sqrt{\pi}\sqrt{\dfrac{e(\varphi-\varphi_i)}{T_{ec}}}} & \text{for} \quad (1-\alpha_e)\leqslant 0 \end{cases} \\ \quad \text{in case of} \quad \dfrac{e(\varphi-\varphi_i)}{T_{ec}} \gg 1. \end{cases} \tag{3}$$

Here the assumptions

$$\frac{e(\varphi-\varphi_b)}{T_{ec}} \gg 1, \quad \frac{\mu_{e**}B_i}{T_{ec}} \gg 1, \tag{4}$$

were made to obtain Eq. (3) so that the contribution of the passing component of electrons from the inner mirror throat, the first two terms on the right-hand side of Eq. (2), can be neglected. In order for the electron distribution function (1) to not become infinite in the range $B_b \leqslant B \leqslant B_i$, when $\mu \to \infty$ with $\varepsilon = \mu B$, the following relation has to be satisfied:

$$\frac{1-\alpha_e B_i/B}{1-\alpha_e} \geqslant 0,$$

that is,

$$\alpha_e \leqslant B_b/B_i \quad \text{or} \quad \alpha_e > 1. \tag{5}$$

Solving φ as a function of n_e in Eq. (3),

$$e(\varphi-\varphi_i) \simeq \begin{cases} T_{ec}\dfrac{B_i-B}{B_i}\ln\left\{\left(\dfrac{B_i}{B_i-B}\right)^{1/2}\dfrac{B-\alpha_e B_i}{B(1-\alpha_e)}\dfrac{n_e(z)}{n_{ec}}\right\} \\ \quad \text{in case of} \quad 1 \gtrsim \dfrac{B_i}{(B_i-B)}\dfrac{e(\varphi-\varphi_i)}{T_{ec}} \\ \begin{cases} (1-\alpha_e)T_{ec}\ln\left\{\dfrac{B-\alpha_e B_i}{B(1-\alpha_e)^{3/2}}\dfrac{n_e(z)}{n_{ec}}\right\} & \text{for} \quad (1-\alpha_e)>0 \\ T_{ec}\dfrac{1}{\pi}\left(\dfrac{B(\alpha_e-1)}{B_i}\right)^2\left(\dfrac{n_{ec}}{n_e(z)}\right)^2 & \text{for} \quad (1-\alpha_e)\leqslant 0 \end{cases} \\ \quad \text{in case of} \quad \dfrac{e(\varphi-\varphi_i)}{T_{ec}} \gg 1. \end{cases} \tag{6}$$

Now we are looking for a relation of φ on n_e and B in the region $z_b \lesssim z \lesssim z_p$ in Eq. (6), the required relation of which is that the density decreases with z but the electrostatic potential φ increases with z, as shown in Fig. 1. Because the magnetic field B is an increasing function of z around $z = z_p$, a possible candidate for the solution of φ is the top or middle equation in Eq. (6). These top and middle equations in Eq. (6) are the same type of equation, that is, $\varphi(z) = \alpha T_{ec}\ln\{G(B)n_e(z)/n_{ec}\}$, where α is constant and $G(B)$ means a function of B. Therefore, we choose the relation of φ on B and n_e as

$$e(\varphi-\varphi_i) = (1-\alpha_e)T_{ec}\ln\left\{\frac{B-\alpha_e B_i}{B(1-\alpha_e)^{3/2}}\frac{n_e(z)}{n_{ec}}\right\}. \tag{7}$$

Here the constant α_e should satisfy the relation $\alpha_e \leqslant B_b/B_i$.

Equation (7) holds for the condition $e(\varphi-\varphi_i)/T_{ec} \gg 1$ as seen in Eq. (6). However, we apply Eq. (7) to the region $e(\varphi-\varphi_i)/T_{ec} \not\gg 1$ because the essential part of the non-Boltzmann distribution of electrons for the plug potential formation is retained. Equation (7) reduces, on the basis of the thermal barrier potential φ_b, to

$$\begin{aligned} e(\varphi-\varphi_b) &= (1-\alpha_e)T_{ec}\ln\left\{\frac{B-\alpha_e B_i}{B(1-\alpha_e)^{3/2}}\frac{n_e(z)}{n_{ec}}\right\} \\ &\quad -(1-\alpha_e)T_{ec}\ln\left\{\frac{B_b-\alpha_e B_i}{B_b(1-\alpha_e)^{3/2}}\frac{n_{eb}}{n_{ec}}\right\} \\ &= (1-\alpha_e)T_{ec}\ln\left\{\frac{B_b[B-\alpha_e B_i]}{B(z)[B_b-\alpha_e B_i]}\frac{n_e(z)}{n_{eb}}\right\}. \end{aligned} \tag{8}$$

Here $n_{eb} \equiv n_e(z_b)$.

The distribution function of electrons trapped in the plug/barrier mirror cell in Eq. (1) is written as

$$f_e = n_{ec}\left(\frac{m_e}{2\pi T_{ec}}\right)^{3/2}\exp\left\{-\frac{\frac{1}{2}m_e v_\parallel^2}{(1-\alpha_e)T_{ec}} - \frac{\frac{1}{2}m_e v_\perp^2}{\frac{(1-\alpha_e)}{(1-\alpha_e B_i/B_b)}T_{ec}} + \frac{e(\varphi_b-\varphi_i)}{(1-\alpha_e)T_{ec}}\right\}, \tag{9}$$

at $z=z_b$, which is a bi-Maxwellian distribution function with two component temperatures $T_{e\parallel}$, $T_{e\perp}$ parallel and perpendicular to the magnetic field line,

$$T_{e\parallel} = (1-\alpha_e)T_{ec}, \quad T_{e\perp} = \frac{(1-\alpha_e)}{(1-\alpha_e B_i/B_b)}T_{ec}. \tag{10}$$

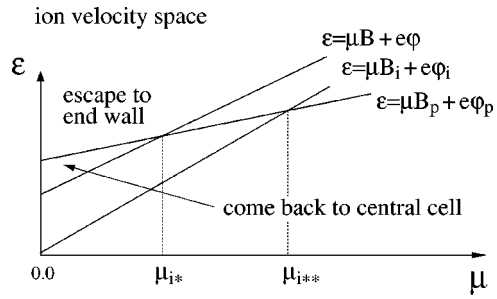

FIG. 2. Ion velocity space represented by ε and μ.

A modified Boltzmann relation (8) is able to be derived on the assumption that the electron distribution function is bi-Maxwellian of Eq. (9) at $z=z_b$ in the whole velocity space, including the region passing to the inner mirror throat $z=z_i$. The electrons coming from the inner mirror throat are fewer at $z=z_b$ than those magnetically trapped in the thermal barrier region, if $B_i/B_b \gg 1$ and $T_{e\perp}/T_{e\parallel} \gg 1$, so that the assumption that the electrons are bi-Maxwellian in the passing region at $z=z_b$ is a good approximation of the Maxwellian electrons in the passing region.

Now we briefly consider the mechanism of a plug potential formation. As mentioned previously in this section, the modified Boltzmann law (8) has a type of $e(\varphi(z)-\varphi_b) = T_{e\parallel}\ln\{G(B)n_i(z)/n_{ec}\}$. Here we assume the charge neutrality condition so that the electron density n_e is the same as the ion density n_i. Because the original scenario of a plug potential formation includes the high energy sloshing ion population, the plug potential is formed at the point where $dn_i/dz=0$ even if $G(B)=1$. In the case of a non-Maxwellian electron distribution in the plug/thermal barrier region, i.e., $G(B)\neq 1$, the plug potential can be formed at the region satisfying $d[G(B)n_i]/dz=0$, if it exists, in the midway from $z=z_b$ to $z=z_m$, even if there is no high energy sloshing ion population.

In order to clarify whether there exists a region where $d[G(B)n_i]/dz=0$, the following ion distribution function is introduced in the region $z_b \leqslant z \leqslant z_m$,

$$f_i = \begin{cases} n_{ic}\left(\frac{m_i}{2\pi T_{ic}}\right)^{3/2}\exp\left\{-\frac{\varepsilon-e\varphi_i}{T_{ic}}\right\} & \text{for } \varepsilon \geqslant \mu B_i + e\varphi_i \\ n_{ic}\left(\frac{m_i}{2\pi T_{ic}}\right)^{3/2}\exp\left\{-\frac{\varepsilon-e\varphi_i-\alpha_i\mu B_i}{(1-\alpha_i)T_{ic}}\right\} & \text{for } \varepsilon < \mu B_i + e\varphi_i \\ 0 \quad \text{for} \begin{cases} v_\parallel \leqslant 0 \\ \text{and} \quad \varepsilon \geqslant \mu B_p + e\varphi_p \\ \text{and} \quad \varepsilon \geqslant \mu B_i + e\varphi_i. \end{cases} \end{cases} \tag{11}$$

Here the ion distribution function is the same type as that of the electron distribution function, and α_i is constant. The ion distribution function in the loss cone in the region $v_\parallel \leqslant 0$ is assumed to be zero, i.e., ions escaping through the outer mirror throat $z=z_m$ never come back again, where we assume $B_m=B_i$ and $\varphi_m=\varphi_i$ for simplicity. The velocity $v_\parallel$ is defined in Sec. III [see Eq. (15)].

Figure 2 plots the diagram of ion velocity space, where

$\mu_{i*} \equiv -e(\varphi-\varphi_p)/(B-B_p)$ and $\mu_{i**} \equiv -e(\varphi_i-\varphi_p)/(B_i-B_p)$. The contribution of ions with the energy $\varepsilon < \mu B_i + e\varphi_i$ to the ion density is neglected assuming $\mu_{i**}B_i/T_{ic} \gg 1$ in the following calculation. The ion density n_i in the region $B \lesssim B_p$ in Fig. 2 is given as

$$n_i(z) = \frac{Bn_{ic}}{\sqrt{\pi}T_{ic}^{3/2}}\left[\frac{1}{2}\int_{\mu B+e\varphi}^{\infty} d\varepsilon \int_0^{\infty} d\mu + \frac{1}{2}\int_{\mu B+e\varphi}^{\mu B_p+e\varphi_p} d\varepsilon \int_0^{\infty} d\mu\right]\frac{1}{(\varepsilon-\mu B-e\varphi)^{1/2}} \times \exp\left\{-\frac{\varepsilon-e\varphi_i}{T_{ic}}\right\}. \tag{12}$$

On the other hand, the ion density in the region $B \gtrsim B_p$ is given as

$$n_i(z) = \frac{Bn_{ic}}{\sqrt{\pi}T_{ic}^{3/2}} \lim_{\mu_{i*}\to\infty}\left[\frac{1}{2}\int_{\mu B_p+e\varphi_p}^{\infty} d\varepsilon \int_0^{\mu_{i*}} d\mu + \frac{1}{2}\int_{\mu B+e\varphi}^{\infty} d\varepsilon \int_{\mu_{i*}}^{\infty} d\mu\right]\frac{1}{(\varepsilon-\mu B-e\varphi)^{1/2}} \times \exp\left\{-\frac{\varepsilon-e\varphi_i}{T_{ic}}\right\}. \tag{13}$$

The integrations in Eqs. (12) and (13) are carried out around $z=z_p$ with the assumption of $0 \leqslant e(\varphi_p-\varphi)/T_{ic} \ll 1$, to be

$$n_i(z) \simeq \begin{cases} \frac{1}{2}n_{ic}\exp\left\{-\frac{e(\varphi_p-\varphi_i)}{T_{ic}}\right\}\left[1+\frac{e(\varphi_p-\varphi)}{T_{ic}}+\left(\frac{B_p-B}{B_p}\right)^{1/2}\right] & \text{for} \quad B \leqslant B_p \\ \frac{1}{2}n_{ic}\exp\left\{-\frac{e(\varphi_p-\varphi_i)}{T_{ic}}\right\}\left(1-\frac{2}{\sqrt{\pi}}\sqrt{\frac{e(\varphi_p-\varphi)}{T_{ic}}}\right) & \text{for} \quad B > B_p \end{cases}. \tag{14}$$

Here the condition that $0 \leqslant -\mu_{i*}B/T_{ic} \ll 1$ is assumed to obtain the ion density in the region $B \leqslant B_p$.

The ion density profile in Eq. (14) indicates that $dn_i/dz = -\infty$ at $z=z_p$ as shown in Fig. 3. A type of modified Boltzmann law $e(\varphi(z)-\varphi_b) = T_{e\parallel}\ln\{G(B)n_i(z)/n_{ec}\}$ in Eq. (8) requires $d[G(B)n_i]/dz = 0$ at the plug. However, Eq. (14) indicates $d[G(B)n_i]/dz = -\infty$ at $\varphi=\varphi_p$ (i.e., $B=B_p$), that is, plug potential does not form. The result of $|dn_i/dz| = \infty$ at $z=z_p$ comes from the fact that $|\partial f_i/\partial\varepsilon| = \infty$ on the line $\varepsilon = \mu B_p + e\varphi_p$ in Eq. (11). This contradiction is avoided by introducing the effect of Coulomb collisions, which makes $|\partial f_i/\partial\varepsilon| < \infty$ on the line $\varepsilon = \mu B_p + e\varphi_p$. The Coulomb collisions, therefore, are expected to make $|dn_i/dz| < \infty$ at $z=z_p$ and so the Coulomb collisions are expected to form the plug potential between $z=z_b$ and $z=z_m$.

III. RESULTS OF MONTE CARLO CALCULATION

In Sec. II it was shown that the ion Coulomb pitch angle scattering, as well as a modified Boltzmann law, was required to form a plug potential. In order to take into account the effect of Coulomb collisions on the ion distribution function, we carry out the Monte Carlo simulation in the following.

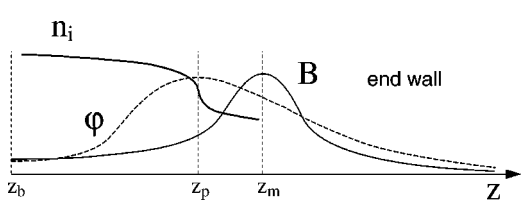

FIG. 3. Schematic diagram of ion density profile around the plug region.

Because the plug potential formation is a one-dimensional problem on z, we calculate the ion orbits along magnetic field line,

$$\frac{dz}{dt} = v_\parallel, \quad v_\parallel = \sqrt{\frac{m_i}{2}(\varepsilon-\mu B-e\varphi)}. \tag{15}$$

Here ε and μ are the ion total energy and magnetic moment, respectively. The ion scattering by Coulomb collision is included by Monte Carlo methods.[21–23] As seen in Figs. 1(a) and 2 the ion velocity space is divided by different mirror trapped regions, so that it is difficult for ions to fill in all regions of velocity space without any collisional effects.

Due to the Coulomb collisions the ions are filled in the thermal barrier region and then finally the ion distribution function becomes Maxwellian. In order to take into account the effects of non-Maxwellian ions in the thermal barrier region in Eq. (11), therefore, the effects of ion (radial) loss are included. That is, an ion loss time τ_L is introduced. The uniform random number ξ_k (which is a number from 0 to 1) is introduced for the kth ion. The number ξ_k is compared with the magnitude of $\exp\{-t_k/\tau_L\}$, where the time t_k is measured from the time when the kth ion was input at the inner mirror throat $z=z_i$ in Fig. 1(a). If $\xi_k > \exp\{-t_k/\tau_L\}$ the kth ion is lost from the plug/barrier mirror cell. Because we are looking for the steady state of plug potential, the ions which are lost are input at the inner mirror throat $z=z_i$ immediately. Here the velocity components $v_\parallel$ and $v_\perp$ of ion at $z=z_i$ are given to be Maxwellian with temperature T_{ic} in the passing region in the velocity space by means of a random number.

On the assumption of charge neutrality condition the electron density is the same as the ion density, i.e., $n_e(z)$

$=n_i(z)$. The electrostatic potential $\varphi(z)$ is determined by the modified Boltzmann law given by Eq. (8). In the simulation the electrostatic potential is given in advance, i.e., $\varphi(z)=0$. The motion of ions is followed in the given electrostatic potential and the density is calculated by each ion position. The calculation of ion motions continues until the steady state of ion density is realized.

The new electrostatic potential is calculated by the modified Boltzmann law (8) with the ion density in the steady state in the old electrostatic potential profile. The ion motion is traced again in the new electrostatic potential profile and the ion density is accumulated after initialized until the steady state of ion density is realized. The above-mentioned procedure is repeated until the steady state of both ion density and electrostatic potential profiles are realized.

The parameters used in the simulation are as follows. The magnetic field profile from $z=z_b$ to $z=z_m$ is adopted for the end-mirror cell in the GAMMA10 tandem mirror,[13] where the axial length L_z from the thermal barrier $z=z_b$ to the outer mirror throat $z=z_m$ is $L_z=120$ cm. The temperatures T_{field} of the field ions and electrons, with which the test ions receive the Coulomb collision, are 100 eV. The number density n_{field}, where the density of field ions is the same as that of field electrons, is $n_{\text{field}}=10^{11}\ \text{cm}^{-3}$, which is uniform along z. In this field plasma the deflection time τ_D is

$$\tau_D=\sqrt{\frac{m_i}{2}}\frac{T_{\text{field}}^{3/2}}{\pi n_{\text{field}} e^4 \ln\Lambda_{ii}}. \tag{16}$$

Here $\ln\Lambda_{ii}$ is the Coulomb logarithm. The time τ_0 is defined as $\tau_0\equiv(T_i/m_i)^{-1/2}$, i.e., the time necessary for a thermal test ion to move by 1 cm, where species of ions is hydrogen.

The temperature of test ions is set $T_i=100$ eV at $z=z_i$. The deflection time is $\tau_D\simeq 5.6\times 10^{-3}$ s and the flight time of 1 cm is $\tau_0\simeq 1.0\times 10^{-7}$ s in above-mentioned parameters. The transit time τ_{transit} of the thermal test ion from $z=z_b$ to $z=z_m$ is $\tau_{\text{transit}}\simeq L_z\times\tau_0\simeq 1.2\times 10^{-5}$ s.

The test ions escaping from the outer mirror throat $z=z_m$ or lost (radially) are input again at the inner mirror throat $z=z_i$ in the simulation. Here the justification of the boundary condition on test ions is mentioned in the following. The ion axial density profile $n_i(z)$ is given by the test ion axial positions as

$$n_i(z)=\sum_k B(z_k)\,\delta(z-z_k). \tag{17}$$

Here z_k is the axial position of the kth test ion and $\delta(\ )$ is the Dirac delta function. The weight $B(z_k)$ in Eq. (17) comes from the fact that the cross section of the magnetic flux tube is in inverse proportion to the magnitude of magnetic field $B(z)$. The total number of ions N_i in the mirror cell from $z=z_b$ to $z=z_m$ in Figs. 1(a) and 3 is given as

$$\begin{aligned} N_i &\equiv \int_{z_b}^{z_m} n_i(z)\frac{dz}{B(z)} \\ &= \int_{z_b}^{z_m}\sum_k B(z_k)\,\delta(z-z_k)\frac{dz}{B(z)} \\ &= \sum_k 1, \end{aligned} \tag{18}$$

where Eq. (17) was used. Therefore, the test ions escaping from the outer mirror throat or radially have to be input immediately at the inner mirror throat in order that the total number N_i does not change in time in the steady state. The above-mentioned boundary condition on test ions means that the ions in the plug/barrier region are supplied by the ion flux from the inner mirror throat.

In order to save computer time, only the region from $z=z_b$ to $z=z_m$ is calculated. The test ions input at $z=z_i$ are mapped at $z=z_b$ with a positive velocity $v_\parallel$ on the assumption of conservation of ε and μ during its flight from $z=z_i$ to $z=z_b$. The test ions reached at $z=z_b$ with $v_\parallel\leqslant 0$ are reflected perfectly at $z=z_b$ if $\varepsilon\leqslant\mu B_i+e\varphi_i$, and are input again at $z=z_i$ with Maxwellian velocity of T_i if $\varepsilon>\mu B_i+e\varphi_i$.

The algorithm of ion supply to the end-mirror cell adopted in the Monte Carlo simulation is consistent with the present tandem mirror experiment, where the ions in the end-mirror cell are supplied from the central cell and escape through the outer mirror throat or escape radially.

The electrostatic potential is set $\varphi_i=0$ at $z=z_i$. The potential φ_b at $z=z_b$ is given in advance and is not changed through simulation run. The potential profile $\varphi(z)$, therefore, is determined on the basis of its magnitude at $z=z_b$.

Figures 4–6 are the steady state test ion distribution functions in the whole axial region represented by ε and μ in the case of $e\varphi_b/T_i=-1$ and $T_{e\perp}/T_{e\parallel}=60$. Here the ion loss time is set at $\tau_L/\tau_0=10^3$ in Fig. 4, $\tau_L/\tau_0=10^4$ in Fig. 5, and $\tau_L/\tau_0=10^5$ in Fig. 6, respectively. The separatrixes denoted by the lines $\varepsilon=\mu B_p+e\varphi_p$ and $\varepsilon=\mu B_m+e\varphi_m$ are determined as the results of the simulation run, while the separatrixes denoted by $\varepsilon=\mu B_i+e\varphi_i$ and $\varepsilon=\mu B_b+e\varphi_b$ are given in advance as boundary conditions of electrostatic potential. It is observed the loss cone in the region $\varepsilon>\mu B_p+e\varphi_p$ and $\varepsilon>\mu B_m+e\varphi_m$ in $v_\parallel<0$ of Figs. 4(b), 5(b) and 6(b). The only velocity space in the region $\varepsilon\geqslant 0$ is plotted in Figs. 4–6, that is, the ions responsible for the plug potential formation, the energy of which is larger than the potential energy $e\varphi_i$ at $z=z_i$, are seen in Figs. 4–6.

Because the ion loss time τ_L is shorter than the deflection time τ_D in Fig. 4, the test ions in the region $\varepsilon\leqslant\mu B_i+e\varphi_i$ are very few. However, the ion distribution function in the passing region from the inner mirror throat $\varepsilon>\mu B_i+e\varphi_i$ is almost independent of μ, i.e., is a part of the Maxwellian distribution function, because the transit time τ_{transit} is shorter than τ_D and τ_L. On the other hand, Fig. 5 is the case of $\tau_L\lesssim\tau_D$, while Fig. 6 is $\tau_L\gtrsim\tau_D$, so that the remarkable increase of ion collisional filling is observed in the region $\varepsilon<\mu B_i+e\varphi_i$ in Fig. 5 to Fig. 6.

The axial profiles of ion density and electrostatic poten-

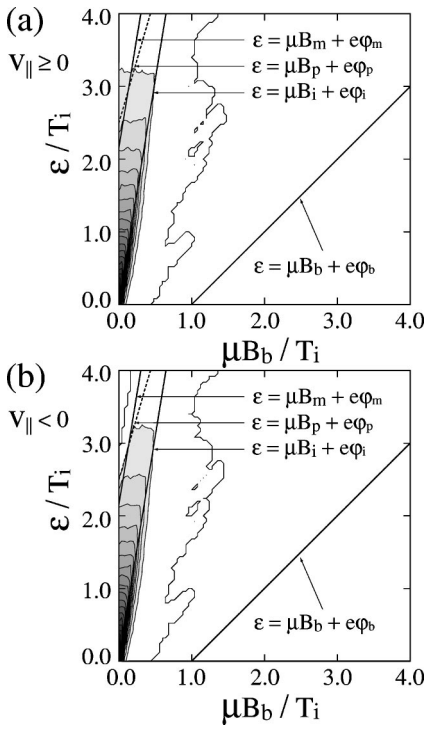

FIG. 4. Ion distribution function represented by ε and μ. The dashed line is $\varepsilon=\mu B_p+e\varphi_p$. Here the parameters used are $e\varphi_b/T_i=-1$, $T_{e\perp}/T_{e\parallel}=60$ and $\tau_L/\tau_0=10^3$. The intervals of each contour are the same as $\delta f=1.5\times10^{-1}$. (a) The velocity space in the region of $v_\parallel\geqslant0$ and (b) that of $v_\parallel<0$.

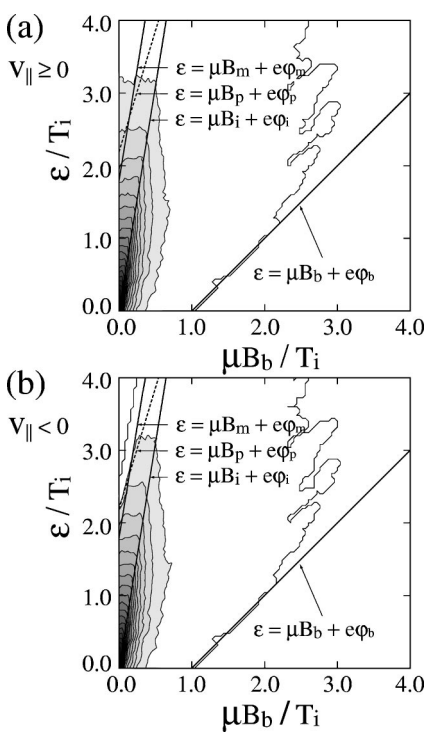

FIG. 5. Ion distribution function represented by ε and μ. The dashed line is $\varepsilon=\mu B_p+e\varphi_p$. Here the parameters used are $e\varphi_b/T_i=-1$, $T_{e\perp}/T_{e\parallel}=60$ and $\tau_L/\tau_0=10^4$. The intervals of each contour are the same as $\delta f=9.4\times10^{-2}$. (a) The velocity space in the region of $v_\parallel\geqslant0$ and (b) that of $v_\parallel<0$.

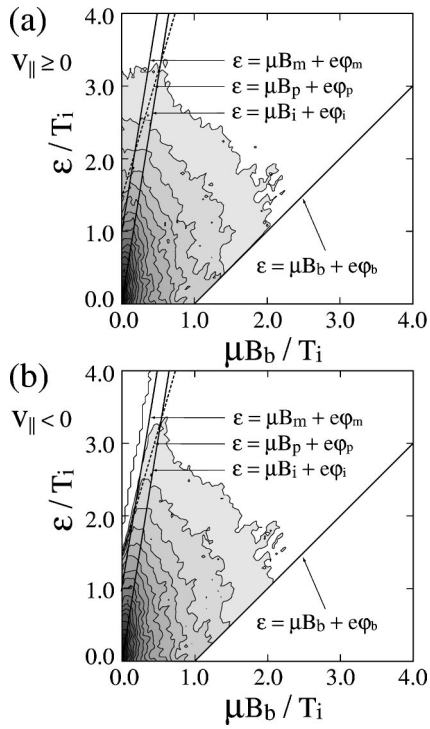

FIG. 6. Ion distribution function represented by ε and μ. The dashed line is $\varepsilon=\mu B_p+e\varphi_p$. Here the parameters used are $e\varphi_b/T_i=-1$, $T_{e\perp}/T_{e\parallel}=60$ and $\tau_L/\tau_0=10^5$. The intervals of each contour are the same as $\delta f=3.5\times10^{-2}$. (a) The velocity space in the region of $v_\parallel\geqslant0$ and (b) that of $v_\parallel<0$.

tial are shown in Fig. 7. Here Fig. 7(a) is $\tau_L/\tau_0=10^3$, Fig. 7(b) is $\tau_L/\tau_0=10^4$, and Fig. 7(c) is the case of $\tau_L/\tau_0=10^5$, which correspond to the simulation results in Figs. 4, 5, and 6, respectively. It is seen that the plug potential (maximum point of the electrostatic potential) is formed in all figures of Figs. 7(a), 7(b), and 7(c).

The maximum point of the ion density profile does not coincide with the position of the plug potential, but rather exists in front of the plug potential, which means almost all ions reflect in front of the plug potential and only a small part of the ions reach the plug point. In the case of few trapped ions in the thermal barrier potential in Figs. 7(a) and 7(b), the peak point of ion density exists around the point where the electrostatic potential is greater than zero, i.e., the point just beyond the height of φ_i. Because the ions have a potential energy $e\varphi_i$ when they are input at $z=z_i$, the ions are reflected extremely by the electrostatic potential when the potential is beyond φ_i. The ion density, therefore, decreases with the growth of the electrostatic potential beyond φ_i. In the case that there exists a large amount of ions trapped in the thermal barrier potential in Fig. 7(c) the peak point of ion density profile is around $z=z_b$.

Figure 8 shows the axial profiles of ion density and electrostatic potential. Here the different parameter in the figures is $T_{e\perp}/T_{e\parallel}$, that is, $T_{e\perp}/T_{e\parallel}=5$ is in Fig. 8(a), $T_{e\perp}/T_{e\parallel}=30$ is in Fig. 8(b), and $T_{e\perp}/T_{e\parallel}=180$ is the case in Fig. 8(c), respectively. The plug potential is found to be formed in Fig. 8 in the wide range of $T_{e\perp}/T_{e\parallel}$. The peak point of the ion density profile is localized around $\varphi=0$ in Figs. 8(b) and

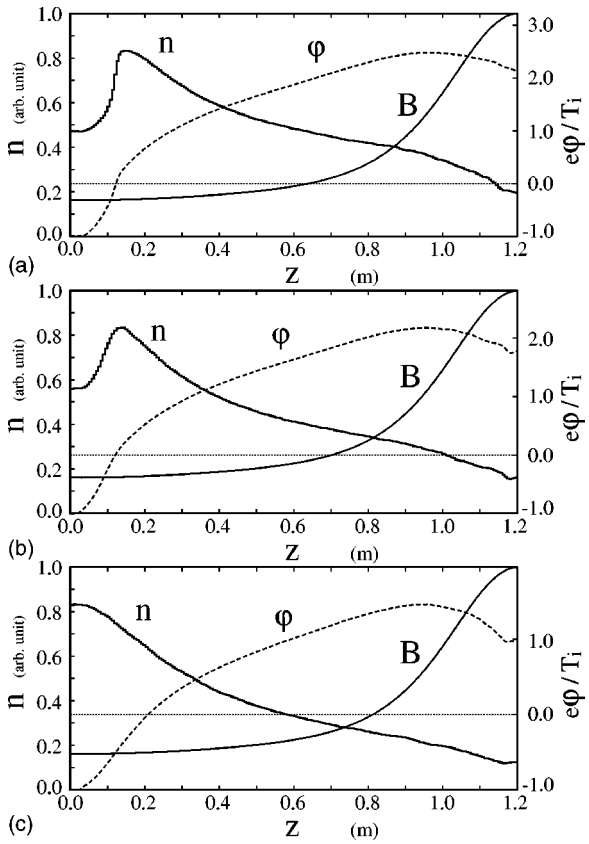

FIG. 7. Axial profiles of ion density n_i and electrostatic potential φ in the magnetic field B from thermal barrier to outer mirror throat. Here the parameters used are $e\varphi_b/T_i=-1$, $T_{e\perp}/T_{e\parallel}=60$. (a) $\tau_L/\tau_0=10^3$, (b) $\tau_L/\tau_0=10^4$, and (c) $\tau_L/\tau_0=10^5$.

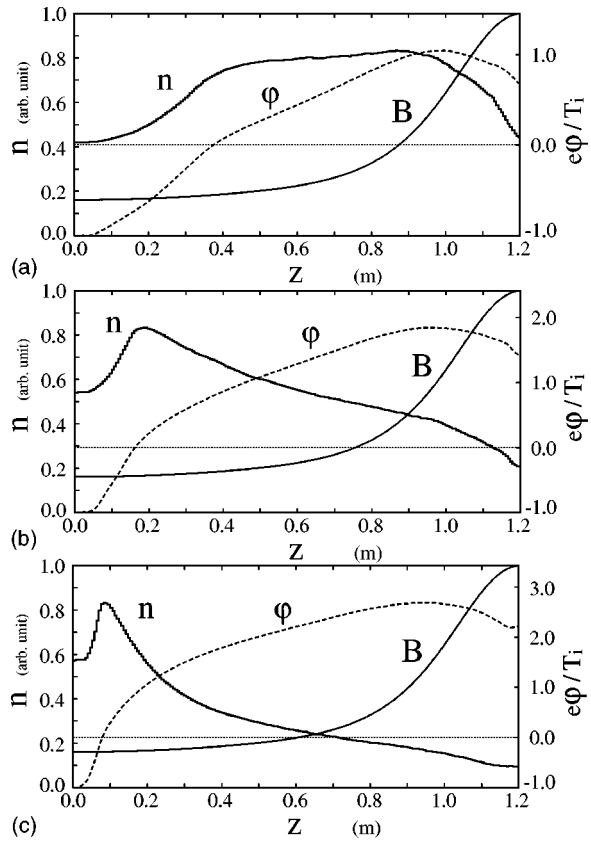

FIG. 8. Axial profiles of ion density n_i and electrostatic potential φ in the magnetic field B from thermal barrier to outer mirror throat. Here the parameters used are $e\varphi_b/T_i=-1$, $\tau_L/\tau_0=10^4$. (a) $T_{e\perp}/T_{e\parallel}=5$, (b) $T_{e\perp}/T_{e\parallel}=30$, and (c) $T_{e\perp}/T_{e\parallel}=180$.

8(c), where almost all ions are reflected by the electrostatic potential before they reach the plug.

Figure 8(a), however, has a different ion density profile from Figs. 8(b) and 8(c). The plug potential height is at most $e\varphi_p/T_i\simeq 1$ in Fig. 8(a). That is, many ions reach the plug without being reflected by the electrostatic potential, in the case of which the ion density profile has a peak around the plug region, because the ion drift velocity along a magnetic field line is retarded by the $\mu\nabla B$ magnetic forces as well as the electrostatic potential in front of the plug region.

Figure 9 plots the height of a plug potential as a function of $T_{e\perp}/T_{e\parallel}$. Here Fig. 9(a) is $e\varphi_b/T_i=-1$, Fig. 9(b) is $e\varphi_b/T_i=-2$, and Fig. 9(c) is the case of $e\varphi_b/T_i=-3$, respectively. The field ion and electron densities and temperatures giving the Coulomb collisions with the test ions are the same as those mentioned previously in this section. The modified Boltzmann law (8) is rewritten by relation (10) as

$$e(\varphi-\varphi_b)=T_{e\parallel}\ln\left\{\left[\frac{T_{e\perp}}{T_{e\parallel}}+\left(1-\frac{T_{e\perp}}{T_{e\parallel}}\right)\frac{B_b}{B(z)}\right]\frac{n_e(z)}{n_{eb}}\right\}. \tag{19}$$

Note that the charge neutrality condition $n_i(z)=n_e(z)$ is assumed through this manuscript. The plug potential is a function of $n_e(z_p)/n_{eb}$ and B_p/B_b as well as $T_{e\perp}/T_{e\parallel}$ in Eq. (19). Figure 9, however, indicates that the height of a plug potential is a function of only $T_{e\perp}/T_{e\parallel}$ as long as τ_D/τ_L is fixed, although the density profile changes greatly by the electrostatic potential in Figs. 7 and 8. All solid lines in Figs. 9(a)–9(c) have the same slope, which is

$$e(\varphi_p-\varphi_i)\simeq 1.1T_{ec}\ln\{T_{e\perp}/T_{e\parallel}\}+g(\tau_L/\tau_D), \tag{20}$$

where $g(\tau_L/\tau_D)$ is a function independent of $T_{e\perp}/T_{e\parallel}$. It is found in Figs. 9(a)–9(c) that the magnitude of $\varphi_p-\varphi_i$ decreases with the increase of $\varphi_b-\varphi_i$, but the magnitude of $\varphi_p-\varphi_b$ increases with the increase of $\varphi_b-\varphi_i$.

Figure 10 shows the magnetic field at the axial position of a plug potential. The position of the plug depends weakly on the ratio $T_{e\perp}/T_{e\parallel}$ and the thermal barrier depth $\varphi_b-\varphi_i$, and the position is almost independent of τ_L/τ_0, i.e., τ_L/τ_D.

IV. SUMMARY AND DISCUSSION

In the Monte Carlo simulation the ion distribution at the inner mirror throat is assumed as Maxwellian, so that the ions lost by end-loss or radial-loss are reinput at the inner mirror throat as part of the Maxwellian from the central cell of a tandem mirror. This procedure of ion supply at the inner mirror throat assumes that the loss cone ($v_\parallel\geqslant 0$) in the velocity space of ions is filled by the Maxwellian ions. In a weakly collisional case and in the absence of microinstabilities, the loss cone is nearly empty and is populated only in a boundary layer near the loss cone boundary.[22,23] Therefore, the solution obtained in this manuscript yields qualitative

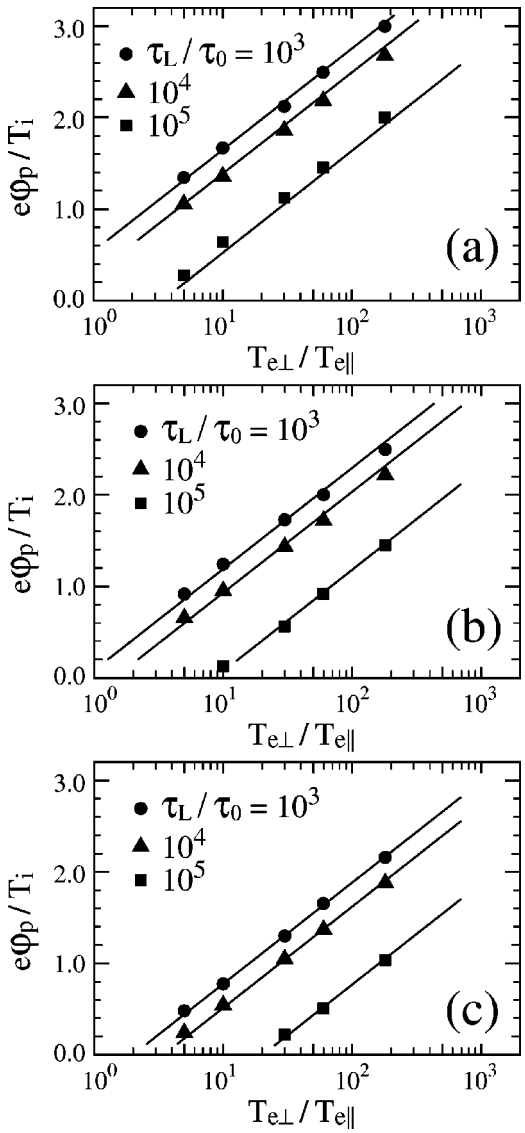

FIG. 9. The height of the plug potential as a function of $T_{e\perp}/T_{e\parallel}$. Here is the case (a) $e\varphi_b/T_i=-1$, (b) $e\varphi_b/T_i=-2$, and (c) $e\varphi_b/T_i=-3$. The symbols denoted by closed circles are the results of simulation with $\tau_L/\tau_0=10^3$, closed triangles are the results with $\tau_L/\tau_0=10^4$, and closed squares are the results with $\tau_L/\tau_0=10^5$.

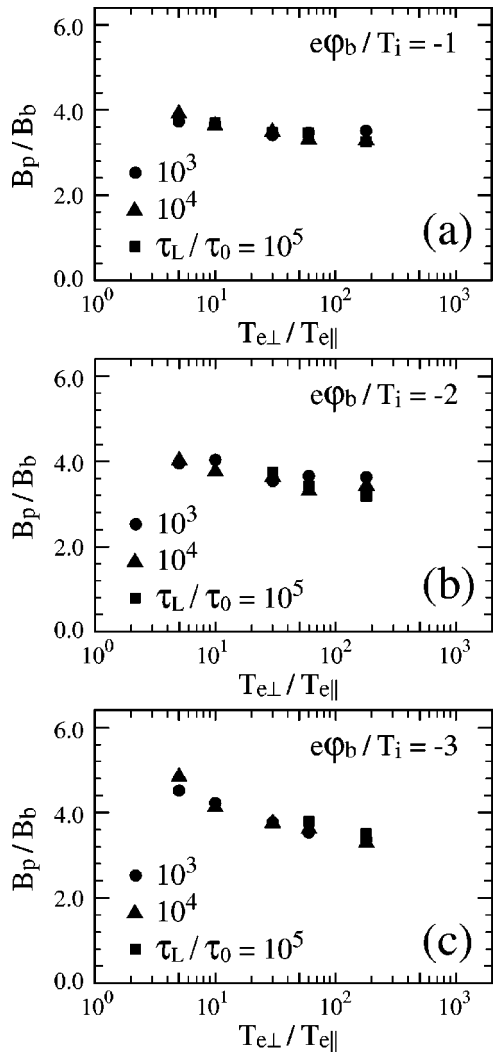

FIG. 10. The axial position represented by B as a function of $T_{e\perp}/T_{e\parallel}$. Here is the case (a) $e\varphi_b/T_i=-1$, (b) $e\varphi_b/T_i=-2$, and (c) $e\varphi_b/T_i=-3$. The symbols denoted by closed circles are the results of simulation with $\tau_L/\tau_0=10^3$, closed triangles are the results with $\tau_L/\tau_0=10^4$, and closed squares are the results with $\tau_L/\tau_0=10^5$.

insights into the plugging process, but will be quantitatively incorrect for a non-Maxwellian central cell case.

We have shown that the plug potential is formed as long as the electron and ion distribution functions are non-Maxwellian in the plug/thermal barrier mirror cell. It is easily shown that there is no solution of φ_p in Eq. (8) if the ions obey the Boltzmann relation, i.e., $n_i=n_{ib}\exp\{-e(\varphi-\varphi_b)/T_i\}$. That is, the plug potential is formed if the modified Boltzmann law $e(\varphi-\varphi_b)=T_{e\parallel}\ln\{G(B)n_e/n_{ec}\}$ applies instead of the traditional Boltzmann law $e(\varphi-\varphi_b)=T_e\ln\{n_e/n_{ec}\}$, and if the ion radial loss exists in addition to the very small ion Coulomb pitch angle scattering into the loss cone region and so the ion distribution function deviates from Maxwellian distribution. The above-mentioned circumstances of plug potential formation are not contradictory to those in the present tandem mirror experiments.[13,14]

The Monte Carlo simulations using the modified Boltzmann law of Eqs. (8) or (19) have led to the results that the magnitude of a plug potential obeys the relation (20). The force to make the ratio $T_{e\perp}/T_{e\parallel}$ large is considered to result from the externally injected microwave power for the fundamental electron cyclotron resonance heating around the plug region. On the other hand, it is known that the larger ratio $T_{e\perp}/T_{e\parallel}$ makes the thermal barrier depth φ_b deeper.[24,25] Therefore, the results of this manuscript, that the plug potential formation requires a non-Maxwellian electron distribution at the thermal barrier, is consistent with the experimental results in which the plug potential formation accompanies the thermal barrier potential formation.[20]

As mentioned in Sec. II the ion population in the loss cone region in the velocity space is required for the plug potential formation. Otherwise dn_i/dz becomes infinity at the potential maximum, as is shown in Fig. 3 schematically. The amount of this ion population in the loss cone region can be very small for the plug potential to form, as long as the

derivative of the ion distribution becomes continuous across the loss cone boundary.

[1]H. Alfvén and C.-G. Fälthammar, *Cosmical Electrodynamics*, 2nd ed. (Oxford University Press, New York, 1963), p. 163.
[2]Y. Serizawa and T. Sato, Geophys. Res. Lett. **11**, 595 (1984).
[3]H. Washimi and I. Katanuma, Geophys. Res. Lett. **13**, 897 (1986).
[4]H. Washimi and I. Katanuma, J. Phys. Soc. Jpn. **62**, 372 (1993).
[5]S. Ishiguro, Y. Kishi, and N. Sato, Phys. Plasmas **2**, 3271 (1995).
[6]See, for example, R. C. Davidson, *Physics of Nonneutral Plasmas* (World Scientific, Singapore, 2001), Chap. 4.
[7]G. Gabrielse, S. L. Rolston, L. Haarsma, and W. Kells, Phys. Lett. A **l29**, 38 (1988).
[8]M. H. Holzscheiter and M. Charlton, Rep. Prog. Phys. **62**, 1 (1999).
[9]Y. Chang and C. A. Ordonez, Phys. Rev. E **62**, 8564 (2000).
[10]D. E. Baldwin and B. G. Logan, Phys. Rev. Lett. **43**, 1318 (1979).
[11]T. C. Simonen, S. L. Allen, T. A. Casper *et al.*, Phys. Rev. Lett. **50**, 1668 (1983).
[12]D. P. Grubb, S. L. Allen, T. A. Casper *et al.*, Phys. Rev. Lett. **53**, 783 (1984).
[13]T. Tamano, Phys. Plasmas **2**, 2321 (1995).
[14]R. S. Post, K. Brau, J. Casey, X. Chen, J. Coleman, H. R. Garner, M. Gerver, S. Golovato, D. Goodman, W. Guss, S. Hiroe, S. Hokin, S. Horne, J. Irby, J. Kesner, B. Lane, T. Morgan, L. Pócs, E. Sevillano, D. Smatlak, D. K. Smith, J. Sullivan, R. P. Torti, and X. Z. Yao, in *Plasma Physics and Controlled Nuclear Fusion Research 1986, Proceedings of the 11th International Conference, Kyoto, 1986* (IAEA, Vienna, 1987), Vol. 2, p. 251.
[15]T. Kaneko, R. Hatakeyama, and N. Sato, Phys. Rev. Lett. **80**, 2602 (1998).
[16]I. Katanuma, Y. Kiwamoto, Y. Tatematsu, K. Ishii, T. Saito, K. Yatsu, and T. Tamano, Phys. Plasmas **3**, 2218 (1996).
[17]T. Saito, I. Katanuma, T. Aota, L. G. Bruskin, T. Cho, M. Hirata, H. Hojo, M. Ichimura, K. Ishii, A. Itakura, N. Katsuragawa, Y. Kiwamoto, J. Kohagura, A. Mase, Y. Nakashima, Y. Sakamoto, M. Shoji, T. Tamano, Y. Tatematsu, T. Tokuzawa, K. Yatsu, M. Yoshikawa, and Y. Yoshimura, Fusion Energy **2**, 105 (1997).
[18]I. Katanuma, Y. Kiwamoto, Y. Tatematsu, K. Ishii, T. Saito, K. Yatsu, and T. Tamano, Phys. Plasmas **4**, 2532 (1997).
[19]I. Katanuma, Y. Kiwamoto, Y. Tatematsu, K. Ishii, T. Saito, T. Tamano, and K. Yatsu, Phys. Plasmas **5**, 1560 (1998).
[20]See, for example, T. Cho, M. Ichimura, M. Inutake, K. Ishii, A. Itakura, I. Katanuma, Y. Kiwamoto, A. Mase, S. Miyoshi, Y. Nakashima, T. Saito, K. Sawada, D. Tsubouchi, N. Yamaguchi, and K. Yatsu, in Ref. 14, p. 243.
[21]I. Katanuma, Y. Kiwamoto, M. Ichimura, T. Saito, and S. Miyoshi, Phys. Fluids B **2**, 994 (1990).
[22]R. Minai, I. Katanuma, and T. Tamano, J. Phys. Soc. Jpn. **66**, 2051 (1997).
[23]R. Minai, I. Katanuma, T. Tamano, and K. Yatsu, J. Phys. Soc. Jpn. **67**, 876 (1998).
[24]I. Katanuma, Y. Kiwamoto, K. Ishii, and S. Miyoshi, Phys. Fluids **29**, 4138 (1986).
[25]I. Katanuma, Y. Kiwamoto, K. Sawada, and S. Miyoshi, Phys. Fluids **30**, 1142 (1987).